

Polarimetric Calibration for Ground-based Synthetic Aperture Radar based on Point Target Approach

NURUL CHASANAH¹, DADANG GUNAWAN¹, FAROHAJI KURNIAWAN², AGUS WIYONO², JEFRI ABNER², BAMBANG SETIADI³

¹Department of Electrical Engineering, Universitas Indonesia, Depok, Indonesia

²Research Center for Aeronautics Technology, BRIN, Bogor, Indonesia

³Research Center for Telecommunication, BRIN, Bogor, Indonesia

Email: nurul.chasanah31@ui.ac.id

*Corresponding author: guna@eng.ui.ac.id

Received 1 September 2024 | Revised 30 September 2024 | Accepted 30 Oktober 2024

ABSTRAK

Kalibrasi polarimetri (PolCal) dari citra radar aperture sintesis berbasis darat (GB SAR) sangat penting dalam aplikasi analisis spasial empiris. Studi ini menyajikan prosedur pra-pemrosesan dan metode kalibrasi untuk memperoleh citra kompleks polarisasi tunggal dengan kualitas tinggi yang terkalibrasi. Pemrosesan data GB SAR menjadi citra kompleks tunggal diterapkan dalam riset ini. Penelitian ini bertujuan untuk menerapkan kalibrasi polarimetri eksternal pada radar gelombang kontinu frekuensi bertahap (SFCW) di pita frekuensi C yang dihasilkan oleh perangkat VNA menggunakan satu trihedral dan dua dihedral CR dengan sudut kemiringan yang berbeda. Setelah pra-pemrosesan, teknik kalibrasi yang diterapkan menunjukkan ketidakseimbangan saluran antara saluran polarisasi yang berbeda (co-pol and cross-pol) dapat diatasi dengan baik.

Kata kunci: Kalibrasi Polarimetri, Radar Apertur Sintesis Berbasis Darat (GB SAR), Ketidakseimbangan Saluran

ABSTRACT

Polarimetric calibration (PolCal) of ground-based synthetic aperture radar (GB SAR) images is critical in empirical spatial analysis applications. This study provides the preprocessing procedures and calibration method required for obtaining high-quality calibrated polarimetric single-look complex imagery. The technique of converting GB SAR data into single-look complex images is examined. This work aimed to perform an external polarimetric calibration of the C-band stepped-frequency continuous wave (SFCW) radar produced by VNA employing single trihedral and two dihedral CRs with varying tilt angles. After preprocessing, the calibration technique profoundly enhances channel imbalance between different polarization channels (co-pol and cross-pol).

Keywords: Polarimetric Calibration, Ground-based synthetic aperture radar (GB SAR), Channel Imbalance

1. INTRODUCTION

Recently, the development of SAR technology has evolved immensely, leading to its widespread application in different areas such as terrain mapping, astronomy, and military surveillance (**Feng et al., 2022**) (**Peters et al., 2021**) (**Song et al., 2022**). Due to its principle of using microwave sensors, SAR offers day and night, all-weather conditions, and high-resolution images (**Richards et al., 2013**). In general, synthetic aperture radar (SAR) is an imaging radar that detects wideband echoes at multiple locations while the platform moves relative to the target. After an accumulating period, SAR produces a two-dimensional (2D) image of the target by processing received echoes coherently, enabling high-resolution scrutiny of the actual image (**Lu, 2019**).

Polarization, the key characteristic of electromagnetic waves, may emit various scattering properties when interacting with ground targets. By analyzing phase and amplitude information from four-channel data using polarimetric decomposition and classification techniques, SAR data can reveal scattering mechanisms on the ground surface caused by distinct objects (**Kirkpatrick et al., 2003**) (**Zhang et al., 2024**). However, polarimetric distortions in SAR data, known as distortion matrices (DMs), may contribute to incorrect inputs and misperception of scattering and ground targets owing to non-ideal system polarization quality and propagation variables (**Jung & Park, 2018**). The major polarimetric distortions relate to channel imbalance, crosstalk, and Faraday rotation errors (**Babu et al., 2022**). The misalignment in the transmit-receive modules (TRMs) and other antenna elements contributes to the vertical component being more vulnerable to horizontal polarization (and vice versa), leading to crosstalk faults. These mistakes contribute to the rising magnitude of cross-pol images, resulting in distortion of volume scattering parameters (**Chang et al., 2018**). Second, the disparity in gain of power amplifiers (PA) between horizontal and vertical polarizations of the same and different TRMs, the distinction in sidelobe lowering capacity of Low Noise Amplifiers (LNA), and the variations in attenuator ways between horizontal and vertical polarizations can lead to channel imbalance and phase bias. Also, a Faraday rotation mistake emerges when a linearly polarized electromagnetic wave propagates through the Earth's ionosphere, solely affecting spaceborne SAR systems (**Kumar et al., 2022**). Therefore, the benefits of polarimetric properties can only be fully realized by rigorous polarimetric calibration, a vital preprocessing procedure that yields exact polarimetric properties.

Mainly, polarimetric calibration schemes are typically classified into three different kinds: corner reflector (CR) calibration (**Freeman et al., 1990**) (**Liang, 2020**), distributed targets (DT) calibration (**Chang et al., 2023**) (**Han et al., 2023**) (**Zhou et al., 2022**), and hybrid calibration employing both CR and DT (**Hou et al., 2022**) (**Quegan, 1994**) (**Tan & Hong, 2016**). The methods that use distributed targets usually require certain assumptions and accurate measurements. Thus, these assumptions will result in a lower calibration accuracy. In the first method, polarimetric distortions are evaluated using artificial calibrators, which might be a polarimetric active radar calibrator (PARC), which is commonly utilized in spaceborne and airborne SAR systems (**Shi et al., 2020**) or passive corner reflectors used as point targets. Besides, the point target method is precise, objective, and has the advantages of lower cost and simple maintenance (**Yu et al., 2022**).

Utilizing the SAR idea of sensor antenna motion, Ground-based synthetic aperture radar (GB SAR) is a type of terrestrial remote sensing that practically expands the sensor antenna aperture by collecting radar signals from various points along its trajectory (**Chasanah et al., 2023**). Contrary to satellite or aerial SAR systems, it is predominantly used for operations requiring precise and steady observations, like surface deformation, monitoring of dams and landslides, and stability evaluation (**Qi et al., 2024**). Moreover, Ground-based SAR (GB SAR) sensors are appropriate for replacing orbital-based solutions since this technique is suitable for

monitoring smaller areas, such as city buildings or mountain hillsides. The sensor platform has advantages such as robustness, swift reassessing time, ideal spatial resolution, and flexibility in adjusting the illumination angle to the peculiar site geometry (**Iglesias et al., 2014**). Provided that the Research Centre for Aeronautics, Indonesia, is developing a GB SAR system to acquire data using a full polarimetric strip map. Therefore, polarimetric calibration needs to be applied to get minimum distortion images.

Table 1 summarizes research on polarimetric calibration for GB SAR. The majority of earlier research used frequency-modulated continuous wave (FMCW) radar. Polarimetric calibration for GB SAR has been developed using a hybrid corner reflector using three types of calibration targets, i.e., trihedral, dihedral, and 22.5°-rotated dihedral corner reflectors without an assumption in FMCW signal that performs at Ku-band (**Wang et al., 2021**). In (**Izumi et al., 2017**), the evaluation of the two calibration procedures by Wiesbeck et al. (**Wiesbeck & Riegger, 1991**), and Gau et al. (**Gau & Burnside, 1995**) was determined to be implemented in circularly polarized GB SAR at C-band using stepped-frequency continuous wave (SFCW) signal. In brief, a study calibration for linearly-polarized (LP) GB SAR in SFCW mode is necessary for improved use in GB SAR. The contribution of this article is that the distortion matrices are calculated concerning the calibration set in the experiment. The calibrator set consists of three calibration targets, i.e., trihedral, dihedral, and 45° rotated dihedral corner reflector in the C band using SFCW signal mode. Then, the polarimetric calibration method (**Wang et al., 2021**) is adapted, making calibrated polarimetric GB SAR in SFCW mode that is simple and quick yet requires no assumptions.

Table 1. Polarimetric Calibration Technique for GB SAR that are described in literature

Ref	Year	Radar Type	Pol	Method
(Krasnov et al., 2023)	2023	FMCW	Linear	Rotating dihedral
(Wang et al., 2021)	2021	FMCW	Linear	GCT
(Baffelli et al., 2018)	2018	FMCW	Linear	STCT
(Sun et al., 2017)	2017	FMCW	N/A	GCT
(Izumi et al., 2017)	2017	SFCW	Circular	GCT
Proposed Research		SFCW	Linear	GCT

The subsequent contents are organized as follows. Section 2 provides a concise overview of the SFCW radar employed in this investigation, along with the calibration technique. Section 3 presents experimental studies conducted to validate the calibration technique. Section 4 proceeds with the analysis and discourse of the gathered data. In conclusion, Section 5 presents the findings.

2. METHOD

2.1 SFCW Radar Signal

A fundamental necessity to produce calibrated polarimetric data is the availability of correctly processed Single Look Complex (SLC) images for all elements of the polarimetric scattering matrix. Therefore, it is vital to understand how data is received from the GB SAR system. The signal in the present research is generated using a vector network analyzer (VNA) as a measurement device. It operates in the frequency domain and employs the stepped-frequency continuous-wave (SFCW) radar principle to obtain the scattering parameter (S_{21}).

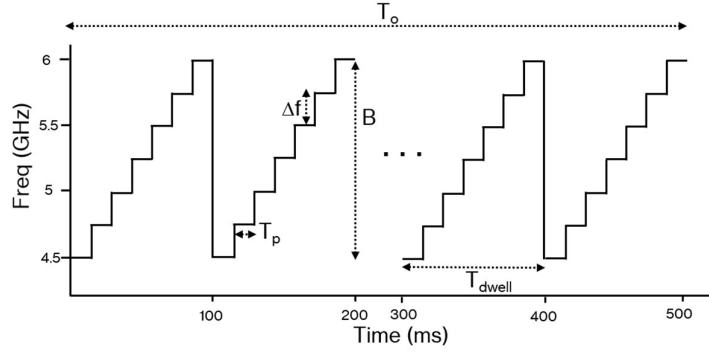


Figure 1. Transmitted signals of SFCW radar

VNA operating in SFCW is depicted in Figure 1. Its sweep time, T_{dwell} , can be defined as the span within the transmission frequency. For (N) frequency points, the frequency rises in Δf increments. The observation time (T_o), or coherent processing time, is the entire duration of all sequential sweeps, whereas the pulse repetition interval T_p is the period of every single step. Sweeping period (T_{dwell}), bandwidth (B), target range (R), and wave speed (c) define the correct sampling frequency. The sampling frequency has to meet or exceed the maximum frequency of baseband signals (**Acar et al., 2021**). The maximum frequency of return signals (F_{max}), is specified as

$$F_{max} = \frac{2BR_{max}}{cT_{dwell}} \quad (1)$$

where the maximum range (R_{max}) should be equal to or less than the unambiguous range, which is

$$R_{max} \leq R_u = \frac{c}{2\Delta f} \quad (2)$$

Another crucial aspect of an SFCW signal is range resolution. The range resolution is referred to as the smallest discernible difference between the radial distances among several targets. The range resolution (ΔR) of an SFCW radar can be measured by

$$\Delta R = \frac{c}{2B} \quad (3)$$

The transmitting signal can be described as

$$S_i(t) = A_i \cos [2\pi(f_0 + i\Delta f)t + \theta_i] \quad (4)$$

$$i = 0, 1, \dots, N - 1$$

In Eq.4, A represents the amplitude, and θ_i represents the phase at step i . Then, receiving signals are delayed types of transmitting signals. The time delay (τ_t) is defined as

$$\tau(t) = \frac{R+x(t)}{c/2} \quad (5)$$

Where (c) is the wave velocity, (R) is the range, and $x(t)$ is the object displacement. The objects' range and displacement are retrieved from baseband return signals of subsequent sweeps. Afterward, the back-projection algorithm (BPA) will readily apply to the received raw data SAR for all polarizations. The procedure consists of two fundamental stages: the inverse FFT is fitted to every row of the complex data matrix to create the synthetic range matrix.

Next, interpolation is implemented to optimize object detection and display the SAR image (Chasanah et al., 2023).

2.2 Polarimetric GB SAR Distortion Model

This research deploys two LP horn antennas in a quasi-monostatic set-up, collecting a single polarization each time utilizing transmitter and receiving antenna sets. Hence, crosstalk calibration is unnecessary because the radar has desirable polarization isolation. The only potential contributor to crosstalk is when the main lobe and cross-polarized antenna sidelobes are pointed in the same direction.

The backscattering characteristics of a ground scatterer can be properly represented by the scattering matrix constructed in the horizontal (H) and vertical (V) polarization patterns as

$$[S] = \begin{bmatrix} S_{hh} & S_{hv} \\ S_{vh} & S_{vv} \end{bmatrix} \quad (6)$$

While first letter of the subscript denotes the scattered or received polarization; the second letter denotes the incident or transmit polarization.

Polarimetric erroneous may affect the scattering coefficients observed by the polarimetric synthetic aperture radar (PolSAR) system. These faults are divided into three distinct kinds: crosstalk, channel imbalance in cross and co-polarization, and Faraday rotation. The Faraday rotation error can be omitted for C-band Pol-SAR (Wright et al., 2003), whereas crosstalk is excluded since we simply get a single polarization at each measurement. The correlation of the measured scattering matrix $[S^m]$ and the right target scattering matrix $[S^c]$ is indicated as

$$[S^m] = [I] + [R][S^c][T] \quad (7)$$

Equation (7) can be expanded as

$$\begin{bmatrix} S_{hh}^m & S_{hv}^m \\ S_{vh}^m & S_{vv}^m \end{bmatrix} = \begin{bmatrix} I_{hh} & I_{hv} \\ I_{vh} & I_{vv} \end{bmatrix} + \begin{bmatrix} R_{hh} & R_{hv} \\ R_{vh} & R_{vv} \end{bmatrix} \begin{bmatrix} S_{hh}^c & S_{hv}^c \\ S_{vh}^c & S_{vv}^c \end{bmatrix} \begin{bmatrix} T_{hh} & T_{hv} \\ T_{vh} & T_{vv} \end{bmatrix} \quad (8)$$

Where $[R]$ is the received errors. $[I]$ is the additive matrix, and $[T]$ is the transmit errors. During polarization calibration, the effects of additive white noise, $[I]$, are usually ignored. Therefore, the equation can be simplified while matrix $[R]$ and $[T]$ can be multiplied into vector form, as follows:

$$\begin{bmatrix} S_{vv}^m \\ S_{hh}^m \\ S_{vh}^m \\ S_{hv}^m \end{bmatrix} = \begin{bmatrix} R_{vv}T_{vv} & R_{vh}T_{hv} & R_{vv}T_{hv} & R_{vh}T_{vv} \\ R_{hv}T_{vh} & R_{hh}T_{hh} & R_{hv}T_{hh} & R_{hh}T_{vh} \\ R_{vv}T_{vh} & R_{vh}T_{hh} & R_{vv}T_{hh} & R_{vh}T_{vh} \\ R_{hv}T_{vv} & R_{hh}T_{hv} & R_{hv}T_{hv} & R_{hh}T_{vv} \end{bmatrix} \begin{bmatrix} S_{vv}^c \\ S_{hh}^c \\ S_{vh}^c \\ S_{hv}^c \end{bmatrix} \quad (9)$$

By combining each of the prospective elements of R_{ij} and T_{ij} into one distortion matrix (C_{ij}) we can generate the calculation stated as

$$[S^m] = [C][S^c]$$


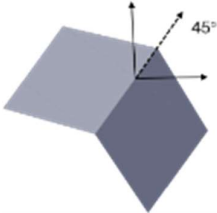

$$\begin{bmatrix} S_{vv}^m \\ S_{hh}^m \\ S_{vh}^m \\ S_{hv}^m \end{bmatrix} = \begin{bmatrix} C_{11} & C_{12} & C_{13} & C_{14} \\ C_{21} & C_{22} & C_{23} & C_{24} \\ C_{31} & C_{32} & C_{33} & C_{34} \\ C_{41} & C_{42} & C_{43} & C_{44} \end{bmatrix} \begin{bmatrix} S_{vv}^c \\ S_{hh}^c \\ S_{vh}^c \\ S_{hv}^c \end{bmatrix} \quad (10)$$

Thus, by sequential substitution of a homogenous system, the sixteen error coefficients of **[C]** can be minimized into eight as follows:

$$\begin{bmatrix} S_{vv}^m \\ S_{hh}^m \\ S_{vh}^m \\ S_{hv}^m \end{bmatrix} = \begin{bmatrix} C_{11} & \frac{C_{32}C_{42}}{C_{44}} & \frac{C_{32}C_{11}}{C_{44}} & \frac{C_{33}C_{42}}{C_{44}} \\ \frac{C_{31}C_{41}}{C_{44}} & C_{22} & \frac{C_{33}C_{41}}{C_{44}} & \frac{C_{31}C_{22}}{C_{44}} \\ C_{11} & C_{22} & C_{11} & C_{33} \\ C_{31} & C_{32} & C_{33} & \frac{C_{32}C_{31}}{C_{44}} \\ C_{41} & C_{42} & \frac{C_{42}C_{41}}{C_{44}} & C_{33} \\ & & C_{44} & C_{44} \end{bmatrix} \begin{bmatrix} S_{vv}^c \\ S_{hh}^c \\ S_{vh}^c \\ S_{hv}^c \end{bmatrix} \quad (11)$$

In principle, those eight unknowns can be ascertained by measuring two or more calibration targets that yield four independently variable backscattering coefficients. The unknown values **C₁₁**, **C₂₂**, **C₃₁**, **C₃₂**, **C₄₁**, and **C₄₂** correspond to the co-pol signals, whereas **C₃₃** and **C₄₄** correspond to the cross-pol signals. For the calibration process, dihedral and triangular trihedral corner reflectors are widely used as calibration point targets due to their known theoretical scattering matrices. Table 2 shows specific information on these calibration corner reflectors.

Table 2. Calibration Target Scattering Matrices Characteristics

Corner Reflectors	Theoretical Scattering Matrices
Vertical Dihedral 	$\begin{bmatrix} 1 & 0 \\ 0 & -1 \end{bmatrix}$
Dihedral 45° 	$\begin{bmatrix} 0 & 1 \\ 1 & 0 \end{bmatrix}$
Triangular Trihedral 	$\begin{bmatrix} 1 & 0 \\ 0 & 1 \end{bmatrix}$

The present study utilized three calibration targets with known scattering matrices **[S^{ci}]** where *i* = 1, 2, and 3 indicate a vertical dihedral, dihedral 45°, and triangular trihedral. As a result, the error coefficients are calculated by solving the equations as follows:

$$C_{11} = \frac{S_{hh}^{c1} S_{vv}^{m3} - S_{hh}^{c3} S_{vv}^{m1}}{S_{vv}^{c3} S_{hh}^{c1} - S_{hh}^{c3} S_{vv}^{c1}} \quad (12)$$

$$C_{32} = \frac{S_{vv}^{c3} S_{vh}^{m1} - S_{vv}^{c1} S_{vh}^{m3}}{S_{vv}^{c3} S_{hh}^{c1} - S_{hh}^{c3} S_{vv}^{c1}} \quad (15)$$

$$C_{22} = \frac{S_{vv}^{c3} S_{hh}^{m1} - S_{hh}^{c1} S_{vv}^{m3}}{S_{vv}^{c3} S_{hh}^{c1} - S_{hh}^{c3} S_{vv}^{c1}} \quad (13)$$

$$C_{41} = \frac{S_{hh}^{c1} S_{hv}^{m3} - S_{hh}^{c3} S_{hv}^{m1}}{S_{vv}^{c3} S_{hh}^{c1} - S_{hh}^{c3} S_{vv}^{c1}} \quad (16)$$

$$C_{31} = \frac{S_{hh}^{c1} S_{vh}^{m3} - S_{hh}^{c3} S_{vh}^{m1}}{S_{vv}^{c3} S_{hh}^{c1} - S_{hh}^{c3} S_{vv}^{c1}} \quad (14)$$

$$C_{42} = \frac{S_{vv}^{c3} S_{hv}^{m1} - S_{vv}^{c1} S_{hv}^{m3}}{S_{vv}^{c3} S_{hh}^{c1} - S_{hh}^{c3} S_{vv}^{c1}} \quad (17)$$

$$c_{33} = \left(\frac{S_{vh}^{m2}}{2S_{vh}^{c2}} \right) \pm \sqrt{\left(\frac{S_{vh}^{m2}}{2S_{vh}^{c2}} \right)^2 - c_{31}c_{32}} \quad (18)$$

$$c_{44} = \left(\frac{S_{hv}^{m2}}{2S_{hv}^{c2}} \right) \pm \sqrt{\left(\frac{S_{hv}^{m2}}{2S_{hv}^{c2}} \right)^2 - c_{41}c_{42}} \quad (19)$$

Finally, the calibrated scattering matrix can be readily acquired after finding the $[C]$ matrix as follows

$$[S^c] = [C]^{-1} [S^m] \quad (20)$$

A flowchart (Fig 2) is presented to make the methods used in this study clear. Since there is no assumption in the calculation, this method can accurately solve imbalance calibration.

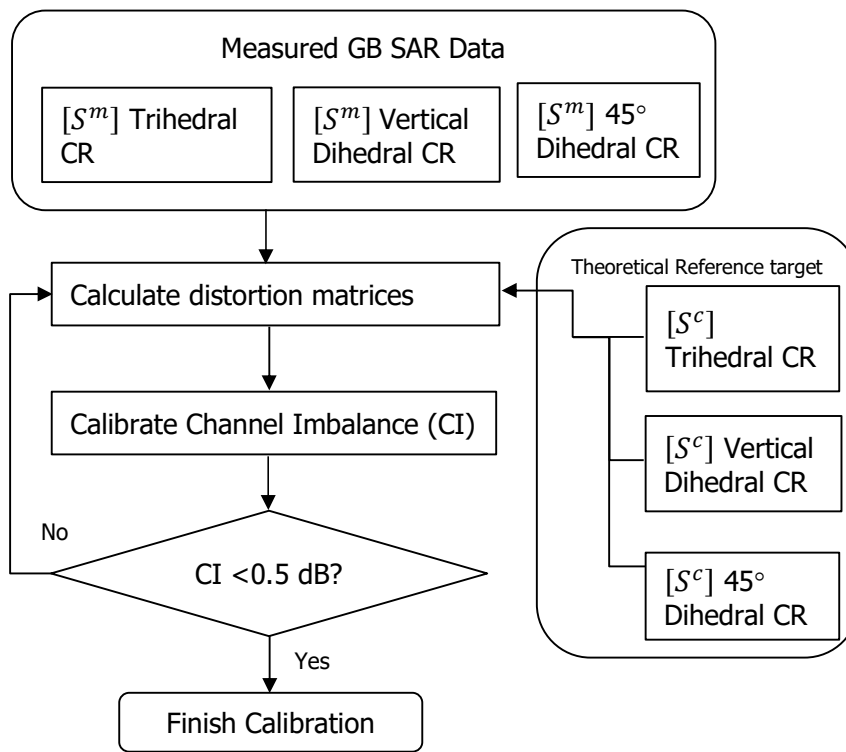


Figure 2. Flowchart of polarimetric calibration procedure from GB SAR data

The technique for calibrating the images from SAR is laid out below.

Step 1: Measure all three reference targets.

Step 2: Compute distortion matrices by adding the theoretical values of the reference targets in (11).

Step 3: Calculate the channel imbalance based on distortion matrices

Step 4: Verify that the polarimetric calibration is applied accurately if the CI is less than 0.5 dB; otherwise, return to Step 2.

2.3 Field Experiment

This section delineates the polarimetric radar measurement configuration employing the quasi-monostatic methodology. A VNA-developed SFCW GB SAR system comprises 1601 sample points and functions within the C-band frequency range of 5-7 GHz. The antenna configuration included a pair of LP horn antennas with a synthetic aperture length of 9 meters and a 10 cm

aperture step in the cross-range. A longer rail scanning distance may lead to better azimuth resolution. However, a lower stepping step is required to avoid multiples caused by azimuth ambiguity. The visual design of the experiment is illustrated in Fig. 3, where one trihedral and two dihedral CRs oriented at 0° and 45° alternatingly were deployed in the open area. Absorbing substances were installed to minimize unwanted echoes from the ground and target position. The target's side dimensions were 30 cm, and the radius between the target and its midsection synthetic aperture antenna was set to 10 meters, allowing for far-field testing. A Laptop can set all the settings, including frequency, output power, and frequency sampling points. Besides, it can control the data acquisition process during the measurements.

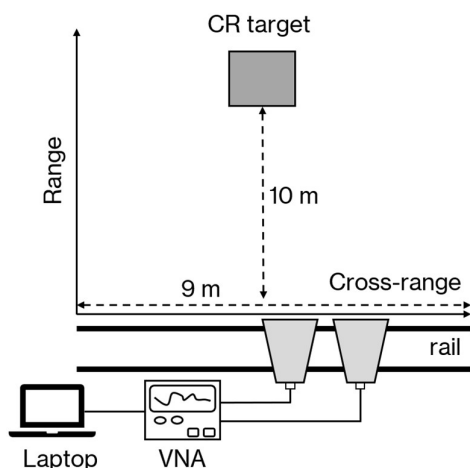


Figure 3. Schematic representation of the GB SAR experiment

3. RESULTS AND DISCUSSION

3.1. SAR Images Processing Results

The SAR images were generated using the back-projection algorithm (BPA). This approach required filtering the range-compressed data around the reflector and converting it back to the time domain using an inverse Fourier transform. Then, the back-projected images were validated by interpolation of the complex data. BPA was preferred for it is the most reliable technique (predicting the matched filter ideal solution) and enables random observation areas. Hence, the retrieved SAR images of the targets for every polarization are shown in Fig. 4-6. The three calibration targets can then be identified in the co-polarimetric images. Nonetheless, all polarimetric signatures demonstrate the 45° -oriented dihedral CR, indicating that the calibration targets were appropriately positioned. The target location can be confirmed from these images as about 10 meters in range direction. Fig. 4 presents the reconstructed images of the trihedral corner reflector in the amplitude domain. Notably, the artificial target constructed of the trihedral is apparent in each case in co-pol signatures ($|S_{VV}|$ and $|S_{HH}|$), with the amplitudes of $|S_{VV}|$ being slightly higher than those of $|S_{HH}|$. Meanwhile, the trihedral target is barely visible in cross-pol signatures ($|S_{VH}|$ and $|S_{HV}|$), and a minor amount of object noise is visible close to the trihedral target.

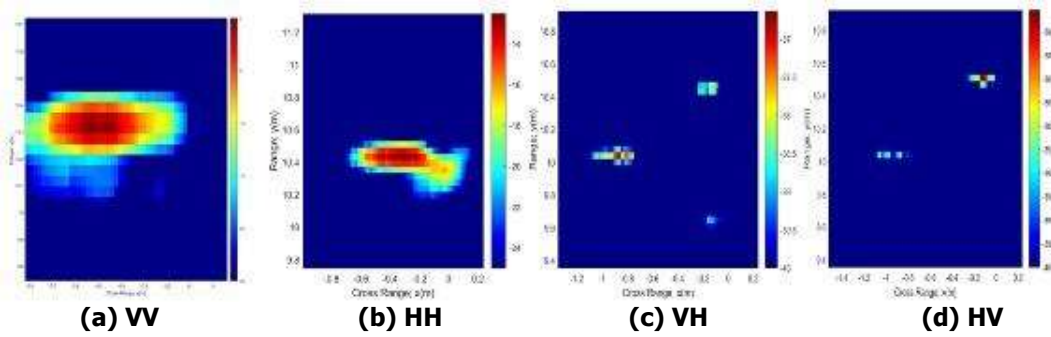


Figure 4. Triangular Trihedral SAR Images

Figure 5 conveys the SAR images in four data channels for vertical dihedral targets. As demonstrated in Fig.5 (c) and (d), the illumination amplitude is roughly -15 dB for cross-pol signatures, while a co-pol signature of about 0 dB demonstrates noteworthy scattering. In principle, assuming a dihedral structure is placed orthogonal to radar illumination, we get notable $|S_{HH}|$ and $|S_{VV}|$ components. Note that the dihedral has an intense co-pol signature and behaves as a double-bounce scatterer when the angle tilts vertically relative to the radar illumination. Meanwhile, the cross-polarized component ($|S_{VH}|$ and $|S_{HV}|$) should not deliver any backscattering signal due to a dihedral placed at 0° only reflecting signal in the identical direction. However, Fig. 5 (c) and (d) illustrate a backscattering signal left in cross-pol images. Therefore, to correct these images, a distortion matrix should be constructed and utilized to calibrate polarimetric GB SAR.

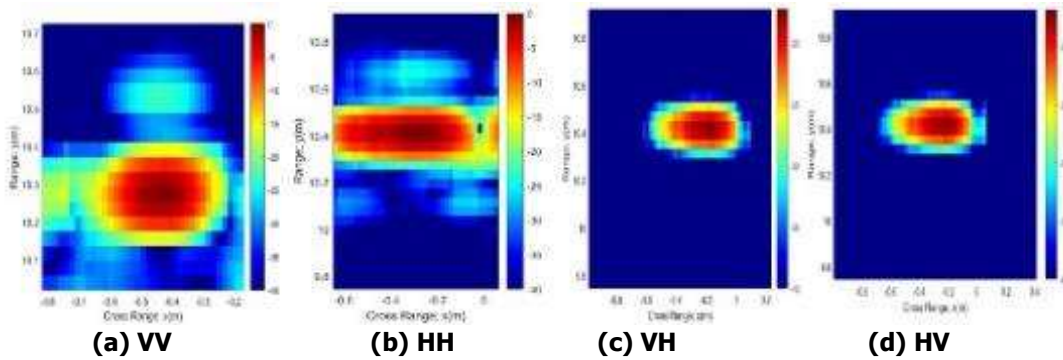


Figure 5. Vertical Dihedral 0° SAR Images

Forests, trees, vegetation, and sloped/oriented surfaces are the primary winding sources of cross-pol SAR images. On top of the 45° -oriented dihedral, there is no straightforward physical representation. Indeed, the dihedral CR is an ideal target for cross-polarization calibration as, while orientated at 45° , the polarization direction shifts from horizontal to vertical direction and vice versa. As a result of polarization alterations, there is no echo of 45° -oriented divedrals in the HH and VV images. Hence, the cross-polarized ($|S_{VH}|$ and $|S_{HV}|$) images highlight the 45° -oriented dihedral. Meanwhile, as shown in Fig. 6 (a) and (b), some backscattering signals in co-pol signatures remain noticeable, with ($|S_{VV}|$) amplitudes being slightly higher than those of ($|S_{HH}|$). The measured $|S_{VH}|$ and ($|S_{HV}|$) images manifest in the first place in magnitude that show 0 dB for its highest value, with ($|S_{VH}|$) amplitudes being slightly greater than those of ($|S_{HV}|$).

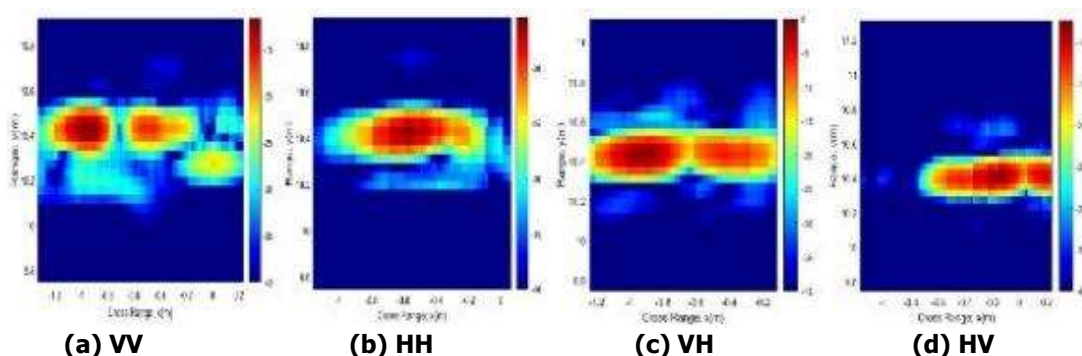


Figure 6. 45° Oriented Dihedral SAR Images

3.2. Polarimetric Calibration

The final polarimetric calibration was carried out using the approach described in Section 2.2, which involved three reflectors in the scene utilized for examining calibration performance. Firstly, the scattering matrices of the target site (the pixel with the highest value) are recovered and normalized to the highest polarization channel value. Table 3 shows the acquired data, reflecting the uncalibrated and calibrated scattering matrices of the three CRs. As calibration targets, these three CRs include a trihedral, a dihedral, and a 45°-oriented dihedral.

Table 3. Scattering Matrix of Three targets before and after calibration

CR	Uncalibrated	Theoretical Value	Calibrated	Amplitude error (dB)
Tri-SVV	1∠102.25	1∠0	0.93∠45.454	0.069
Tri-SHH	0.235∠110.06	1∠0	1.042∠48.182	0.042
Tri-SVH	0.0079∠45.92	0∠0	0.051∠-77.92	0.052
Tri-SHV	0.008∠179.01	0∠0	0.052 ∠102.01	0.052
Di0°-SVV	1∠-7.878	1∠180	1.269∠171.819	0.269
Di0°-SHH	0.4877∠49.181	1∠0	1.1828 ∠37.905	0.183
Di0°-SVH	0.067∠127.22	0∠0	0.03082∠43.0391	0.031
Di0°-SHV	0.0703∠145.906	0∠0	0.0294 ∠132.289	0.029
Di45°-SVV	0.259∠115.05	0∠0	0.2274∠96.19	0.227
Di45°-SHH	0.168∠154.02	0∠0	0.0509 ∠91.187	0.051
Di45°-SVH	1∠113.24	1∠0	0.9863∠0.48	0.0137
Di45°-SHV	0.426∠90.373	1∠0	1.043 ∠1.65	0.043

Table 3 reveals that the amplitude error before polarimetric calibration in $|S_{HH}|$ is 0.765 dB for trihedral and 0.512 dB for vertical dihedral, whereas the amplitude error in $|S_{HV}|$ for 45°-oriented dihedral CR is 0.574 dB. To obtain high-quality polarimetric SAR images, the amplitude error should be less than 0.5 dB. Meanwhile, except for these three polarimetric modes, the amplitude error exceeds the requirement. After polarimetric calibration, the amplitude error shows good performance for all these three conditions that $|S_{HH}|$ is reduced to 0.042 dB for trihedral and 0.183 dB for vertical dihedral, while the amplitude error in $|S_{HV}|$ for 45°-oriented dihedral CR is 0.043 dB.

After polarimetric calibration, the channel imbalance value improved to 0.08 dB for the vertical dihedral target, 0.176 dB for the 45°-oriented dihedral target, and 0.11 dB for the trihedral target. The experiment demonstrates that the technique performs satisfactorily regarding channel imbalance accuracy. Nonetheless, the residual distortion of imbalances persists under

certain circumstances. As considering channel balancing, we aim to preserve the orthogonality of the signals in the copol and cross-pol channels, meaning that the amplitude, phase, and latency differences must be regulated to acquire accurate measurements of the target characteristics. This systemic issue needs to be addressed at the hardware level. However, if the impacts of residual channel imbalance are alleviated afterward, we must address it mathematically by utilizing data-driven approaches. In contrast, the measured phases before and after calibration are near the predicted ones for a 45°-oriented dihedral in cross-pol (0.48° phase error in VH and 1.65° phase error in HV). This result creates a channel phase imbalance of 1.17°. Additional phase values for different targets and polarizations may not be the same theoretically. The occurrence was mostly caused by the impact of the tilt angle GB SAR system, which varied between experiments. It should be noted that the signal phase refers to the number of oscillation cycles of a waveform that go between the radar and surface before returning. As a result, interaction with the ground surface may impact data collection.

Finally, the above analysis shows that polarimetric calibration can be carried out successfully through quasi-monostatic SFCW waveform mode in C band signal, resulting in <0.2 dB channel imbalance in amplitude and meeting calibration requirements. Meanwhile, the residual phase channel imbalance persists and will require phase correction in future research. Furthermore, this study can be enhanced by using polarimetric decomposition to examine the effect of calibration on the obtained images.

4. CONCLUSION

The primary aim of this research is to calibrate polarimetric GB SAR in SFCW mode, which is efficient and straightforward yet eliminates any assumptions. The study focuses on an algorithm incorporating a single trihedral and two dihedral CRs at distinct rotation angles. Calibration accuracy has been shown by examining the scattering matrices of the selected CRs target before and after calibration, revealing significant conformity between calibrated and theoretical polarimetric responses is readily achievable by assuming zero crosstalk. Regarding channel imbalance, the findings suggest that it can be effectively removed with great precision by utilizing the proposed method. The amplitude error tends to be minimized to 0.2 dB. However, the phase error needs to be resolved in future research.

ACKNOWLEDGEMENTS

The authors would like to thank all Synthetic Aperture Radar Research Group members for their help with data preparation and measurement. Also, this research was funded by the Rumah Program Research Centre for Aeronautics Technology, BRIN and the Lembaga Pengelola Dana Pendidikan (LPDP) as part of the Riset dan Inovasi untuk Indonesia Maju (RIIM) program.

REFERENCES

- Acar, Y. E., Saritas, I., & Yaldiz, E. (2021). An S-band zero-IF SFCW through-the-wall radar for range, respiration rate, and DOA estimation. *Measurement*, *186*, 110221. <https://doi.org/10.1016/j.measurement.2021.110221>

- Babu, A., Kumar, S., & Agrawal, S. (2022). Polarimetric Calibration and Spatio-Temporal Polarimetric Distortion Analysis of UAVSAR PolSAR Data. *Earth and Space Science*, *9*(4), e2020EA001629.
- Baffelli, S., Frey, O., Werner, C., & Hajnsek, I. (2018). Polarimetric Calibration of the Ku-Band Advanced Polarimetric Radar Interferometer. *IEEE Transactions on Geoscience and Remote Sensing*, *56*(4), 2295–2311. <https://doi.org/10.1109/TGRS.2017.2778049>
- Chang, Y., Li, P., Yang, J., Zhao, J., Zhao, L., & Shi, L. (2018). Polarimetric Calibration and Quality Assessment of the GF-3 Satellite Images. *Sensors*, *18*(2), 403. <https://doi.org/10.3390/s18020403>
- Chang, Y., Zhao, L., Liu, B., He, H., Fan, J., & Li, P. (2023). Polarimetric Calibration of Airborne SAR Images Using Low Helix Scattering Distributed Targets. *IGARSS 2023 - 2023 IEEE International Geoscience and Remote Sensing Symposium*, 4529–4531. <https://doi.org/10.1109/IGARSS52108.2023.10282499>
- Chasanah, N., Abner, J., Wiyono, A., Rahayu, N., Kurniawan, F., Widada, W., Setiadi, B., & Gunawan, D. (2023). Experimental Evaluation of Polarimetric Ground Based Synthetic Aperture Radar Imaging using Portable VNA. *2023 International Conference on Radar, Antenna, Microwave, Electronics, and Telecommunications (ICRAMET)*, 6–11. <https://doi.org/10.1109/ICRAMET60171.2023.10366606>
- Feng, H., Zhang, L., Dong, J., Li, S., Zhao, Q., Luo, J., & Liao, M. (2022). Mapping the 2021 October Flood Event in the Subsiding Taiyuan Basin by Multitemporal SAR Data. *IEEE Journal of Selected Topics in Applied Earth Observations and Remote Sensing*, *15*, 7515–7524. <https://doi.org/10.1109/JSTARS.2022.3204277>
- Freeman, A., Shen, Y., & Werner, C. L. (1990). Polarimetric SAR calibration experiment using active radar calibrators. *IEEE Transactions on Geoscience and Remote Sensing*, *28*(2), 224–240. <https://doi.org/10.1109/36.46702>
- Gau, J.-R. J., & Burnside, W. D. (1995). New polarimetric calibration technique using a single calibration dihedral. *IEE Proceedings - Microwaves, Antennas and Propagation*, *142*(1), 19-25(6).
- Han, Y., Lu, P., Liu, X., Hou, W., Gao, Y., Yu, W., & Wang, R. (2023). On the Method of Circular Polarimetric SAR Calibration Using Distributed Targets. *IEEE Transactions on Geoscience and Remote Sensing*, *61*, 1–16.
- Hou, W., Zhao, F., Liu, X., Liu, D., Han, Y., Gao, Y., & Wang, R. (2022). Hybrid Compact Polarimetric SAR Calibration Considering the Amplitude and Phase Coefficients Inconsistency. *Remote Sensing*, *14*(2).

- Iglesias, R., Fabregas, X., Aguasca, A., Mallorqui, J. J., Lopez-Martinez, C., Gili, J. A., & Corominas, J. (2014). Atmospheric Phase Screen Compensation in Ground-Based SAR With a Multiple-Regression Model Over Mountainous Regions. *IEEE Transactions on Geoscience and Remote Sensing*, *52*(5), 2436–2449.
- Izumi, Y., Demirci, S., Baharuddin, M. Z., Waqar, M. M., & Sri Sumantyo, J. T. (2017). The Development And Comparison Of Two Polarimetric Calibration Techniques For Ground-Based Circularly Polarized Radar System. *Progress In Electromagnetics Research B*, *73*, 79–93. <https://doi.org/10.2528/PIERB17010604>
- Jung, Y. T., & Park, S.-E. (2018). Comparative Analysis of Polarimetric SAR Calibration Methods. *Remote Sensing*, *10*(12). <https://www.mdpi.com/2072-4292/10/12/2060>
- Kirkpatrick, C. J., Bittinger, F., Nozadze, K., & Wessler, I. (2003). Expression and function of the non-neuronal cholinergic system in endothelial cells. *Life Sciences*, *72*(18), 2111–2116.
- Krasnov, O. A., Zhang, Q., & Yarovoy, A. (2023). Polarimetric Calibration of an FMCW Doppler Radar with Dual-Orthogonal Signals. *2023 IEEE Conference on Antenna Measurements and Applications (CAMA)*, 312–317. <https://doi.org/10.1109/CAMA57522.2023.10352897>
- Kumar, S., Babu, A., Agrawal, S., Asopa, U., Shukla, S., & Maiti, A. (2022). Polarimetric calibration of spaceborne and airborne multifrequency SAR data for scattering-based characterization of manmade and natural features. *Advances in Space Research*, *69*(4), 1684–1714. <https://doi.org/10.1016/j.asr.2021.02.023>
- Liang, W. (2020). A Set of Point-Targets-Based Polarimetric Calibration Methods Based on General Polarimetric System Model. *IEEE Journal of Selected Topics in Applied Earth Observations and Remote Sensing*, *13*, 2502–2519.
- Lu, J. (2019). *Design Technology of Synthetic Aperture Radar*. Wiley. <https://books.google.co.id/books?id=6tOdDwAAQBAJ>
- Peters, S. T., Schroeder, D. M., Haynes, M. S., Castelletti, D., & Romero-Wolf, A. (2021). Passive Synthetic Aperture Radar Imaging Using Radio-Astronomical Sources. *IEEE Transactions on Geoscience and Remote Sensing*, *59*(11), 9144–9159. <https://doi.org/10.1109/TGRS.2021.3050429>
- Qi, Y., Hui, J., Hou, T., Huang, P., Tan, W., & Xu, W. (2024). A Clustering Approach for Atmospheric Phase Error Correction in Ground-Based SAR Using Spatial Autocorrelation. *Sensors*, *24*(13). <https://doi.org/10.3390/s24134240>

- Polarimetric Calibration for Ground-based Synthetic Aperture Radar based on Point Target Approach
- Quegan, S. (1994). A unified algorithm for phase and cross-talk calibration of polarimetric data-theory and observations. *IEEE Transactions on Geoscience and Remote Sensing*, *32*(1), 89–99. <https://doi.org/10.1109/36.285192>
- Richards, M. A., Scheer, J. A., & Holm, W. A. (2013). *Principles of Modern Radar: Basic Principles*. <https://api.semanticscholar.org/CorpusID:114114032>
- Shi, L., Li, P., Yang, J., Sun, H., Zhao, L., & Zhang, L. (2020). Polarimetric calibration for the distributed Gaofen-3 product by an improved unitary zero helix framework. *ISPRS Journal of Photogrammetry and Remote Sensing*, *160*, 229–243. <https://doi.org/10.1016/j.isprsjprs.2019.12.003>
- Song, Y., Li, J., Gao, P., Li, L., Tian, T., & Tian, J. (2022). Two-Stage Cross-Modality Transfer Learning Method for Military-Civilian SAR Ship Recognition. *IEEE Geoscience and Remote Sensing Letters*, *19*, 3162707. <https://doi.org/10.1109/LGRS.2022.3162707>
- Sun, G., Huang, L., Chen, K., & Han, C. (2017). An Efficient Polarimetric SAR Calibration Algorithm Using Corner Reflectors. *Canadian Journal of Remote Sensing*, *43*(3), 286–296. <https://doi.org/10.1080/07038992.2017.1330142>
- Tan, H., & Hong, J. (2016). Calibration of Compact Polarimetric SAR Images Using Distributed Targets and One Corner Reflector. *IEEE Transactions on Geoscience and Remote Sensing*, *54*(8), 4433–4444.
- Wang, S., Chen, K.-S., & Sato, M. (2021). Performance of SAR Polarimetric Calibration Using Hybrid Corner Reflectors: Numerical Simulations and Experimental Measurements. *IEEE Journal of Selected Topics in Applied Earth Observations and Remote Sensing*, *14*, 440–451.
- Wiesbeck, W., & Riegger, S. (1991). A complete error model for free space polarimetric measurements. *IEEE Transactions on Antennas and Propagation*, *39*(8), 1105–1111. <https://doi.org/10.1109/8.97343>
- Wright, P. A., Quegan, S., Wheadon, N. S., & Hall, C. D. (2003). Faraday rotation effects on L-band spaceborne SAR data. *IEEE Transactions on Geoscience and Remote Sensing*, *41*(12), 2735–2744. <https://doi.org/10.1109/TGRS.2003.815399>
- Yu, T., Li, M., Li, W., Mao, H., Wang, R., Hu, C., & Long, T. (2022). Polarimetric Calibration Technique for a Fully Polarimetric Entomological Radar Based on Antenna Rotation. *Remote Sensing*, *14*(7), 1551. <https://doi.org/10.3390/rs14071551>
- Zhang, S., Cui, L., Zhang, Y., Xia, T., Dong, Z., & An, W. (2024). Research on Input Schemes for Polarimetric SAR Classification Using Deep Learning. *Remote Sensing*, *16*(11). <https://doi.org/10.3390/rs16111826>

Zhou, Y., Zhuang, L., Duan, J., Zhang, F., & Hong, W. (2022). Synthetic Aperture Radar Radiometric Cross Calibration Based on Distributed Targets. *IEEE Journal of Selected Topics in Applied Earth Observations and Remote Sensing*, 15, 9599–9612.